Radioactivity Detection: PET and SPECT Scanners

5

What we observe as material bodies and forces are nothing but shapes and variations in the structure of space. Particles are just schaumkommen (appearances). The world is given to me only once, not one existing and one perceived. Subject as well as object is only one. The barrier between them cannot be said to have broken down as a result of recent experience in the physical sciences, for this barrier does not exist. (Erwin Schrodinger)

5.1 Interaction of Radiation with Matter

Radiation emitted by radionuclides can be classified into electromagnetic (such as X-rays, γ-rays, annihilation photons) or particulate (such as β^-, and β^+) radiation. When we speak of the interaction of radiation with matter, we mean its interaction with the electrons, and nucleus of atoms. The interaction of radiation, in general, may be classified as *elastic* or *inelastic*. In an elastic interaction, the incident radiation is scattered in a different direction, but the total energy of the interacting particles is conserved. In contrast, in an inelastic interaction, a certain amount of energy is lost emitted X-rays.

Ionization occurs when an electron is ejected from an atom, producing an ion pair, a free electron, and a positive atom. High-energy photons (X-rays, γ-rays, and annihilation photons) and charged particles (β^-, β^+, H, and α or He^{2+}) are regarded as ionizing radiation. If an electron is not ejected from the atom but merely raised to higher energy levels or outer shells, the process is termed *excitation*, and the atom is said to be *excited*. In certain materials, when the electrons in the excited state drop to a lower energy state, with the emission of visible light, then that material is said to exhibit *luminescence*. If the production of light ceases within 10^{-8} s of the end of irradiation (or interaction), then the process is one of *fluorescence*; if it continues beyond this point, then the process is called *phosphorescence* (also known as *afterglow*).

5.1.1 Interactions of Charged Articles

5.1.1.1 Ionization

Charged particles (such as electrons β^-, β^+, and H^+) passing an absorbing medium transfer some of the energy to electrons of the medium and are then deflected. Therefore, they cause^{++} *ionization* and/or *excitation*. The probability of scattering increases with the atomic number *Z* of the absorbing medium and decreases rapidly with the increasing kinetic energy of the incident electron. In a close encounter, an orbital electron may be separated from the atom, thus causing ionization. The ejected electron may have sufficient energy to cause secondary ionization and eject an orbital electron, known as delta (δ) rays. The *specific ionization* (SI), the number of primary and secondary ion pairs produced per centimeter in air,

S. Vallabhajosula, *Molecular Imaging and Targeted Therapy*,
https://doi.org/10.1007/978-3-031-23205-3_5

at standard temperature and pressure (STP), can be estimated on the basis of the velocity (v) of incident electron and the velocity of light (c) using the following equation:

$$\mathrm{SI} = \frac{45}{(v/c)^2} \tag{5.1}$$

A less close encounter of the incident charged particle with an atom or molecule may result in an orbital electron being raised to an excited state, thus causing atomic or molecular excitation. The energy absorbed by the atom is dissipated in the subsequent atomic emission of electromagnetic radiation (such as infrared, visible, or UV).

5.1.1.2 Bremsstrahlung Radiation

When an incident β^- particle penetrates the electron cloud of an atom, it may interact with the nucleus and may be deflected with a reduced velocity. The energy lost by the incident electron will appear as electromagnetic radiation, known as bremsstrahlung (breaking radiation) (Fig. 5.1). The probability of bremsstrahlung varies with Z^2 of the absorbing medium.

5.1.1.3 Annihilation Radiation

A positron (β^+), after expending its kinetic energy in inelastic collisions, combines with an electron (β^-) of the absorbing medium. Both the particles are annihilated, and their mass appears as electromagnetic radiation (usually two 511-keV photons), known as annihilation radiation (Fig. 5.1). This interaction of β^- and β^+ particles (matter and antimatter) is called *pair annihilation*.

5.1.1.4 Cerenkov Radiation

Particles normally cannot exceed the velocity of light in a vacuum (3.0×10^{10} cm s^{-1}). Light, however, travels at slower speeds in different materials or media. It is possible for β^- rays to travel at speeds much higher than that of light in a specific medium. When this occurs, visible light, known as *Cerenkov radiation*, is emitted. For example, the blue glow seen near the core of a swimming pool reactor is due to Cerenkov radiation.

5.1.2 Interaction of High-Energy Photons

The interaction of electromagnetic radiation with atoms, electrons, and nuclei of different materials is generally regarded as a collision involving transfer of their energy to matter without necessarily causing ionization directly. However, certain interactions do eject orbital electrons, produce ion pairs, and cause ionization effects. Therefore, high-energy photons, similar to charged particles, are regarded as ionizing radiation. However, unlike charged particles, high-energy photons being massless can penetrate

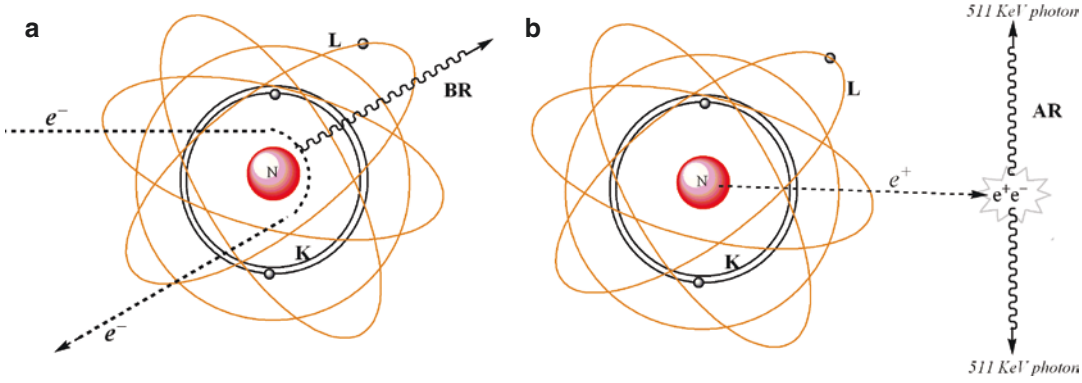

Fig. 5.1 Interaction of charged particles with matter. When high-energy electrons penetrate and approach the nucleus, they are decelerated and deflected (**a**). As a result, bremsstrahlung radiation (BR) is produced. The positron emitted from the atomic nucleus finally interacts with an electron and annihilates it (**b**). As a result, annihilation radiation (AR) is produced in which two photons with a minimum of 511 keV energy travel in opposite directions

soft-tissue thickness of >10 cm in vivo and are considered to be highly penetrating radiation.

The high-energy photons of X-rays, γ-rays, and annihilation radiation associated with radiotracers in nuclear medicine undergo inelastic interactions by means of several mechanisms. The *photoelectric effect* and *Compton scattering* are important in radiation detection and measurement. Pair production and photodisintegration have a high-energy threshold (>1 MeV) and are not relevant to the photon energies normally encountered in nuclear medicine.

5.1.2.1 Photoelectric Effect

When a metal is exposed to electromagnetic radiation, electrons are ejected from the metal (Fig. 5.2). These electrons are called *photoelectrons*. Light with shorter wavelengths (such as UV) ejects electrons with greater speed. Thus, the kinetic energy of photoelectrons is dependent on the frequency; however, the number of electrons ejected depends on the intensity of the electromagnetic radiation. Different metals have different threshold values for the frequency. Depending on the Z of the element, electrons may be held more loosely or tightly. Einstein was able to show that photons with higher energy eject electrons with greater kinetic energy. This phenomenon of the photoelectric effect is very important for the interaction of radiation with matter and for developing radiation detectors. The photoelectric effect should obey the following relationship:

$$h\nu = \mathrm{KE}_{\max} + \varphi \tag{5.2}$$

Where

$$\varphi = h\nu_0 \tag{5.3}$$

Also, ν_0 is the critical frequency below which no photoelectric effect occurs and φ (or ϕ) is the minimum energy (called the *work function* of the metal) needed for the electron to escape from a metal surface. The photoelectric effect is an atomic absorption process in which an atom totally absorbs the energy of the incident photon. It is an interaction of photons with orbital electrons in an atom, mostly the inner-shell electrons, in which the photon transfers all of its energy to the electron, which is then ejected. Some of the energy of the incident photon is used to overcome the binding energy of the electron, and the remaining energy is given to the photoelectron, as kinetic energy. Since the ejection of a photoelectron creates a vacancy in the inner shell, the

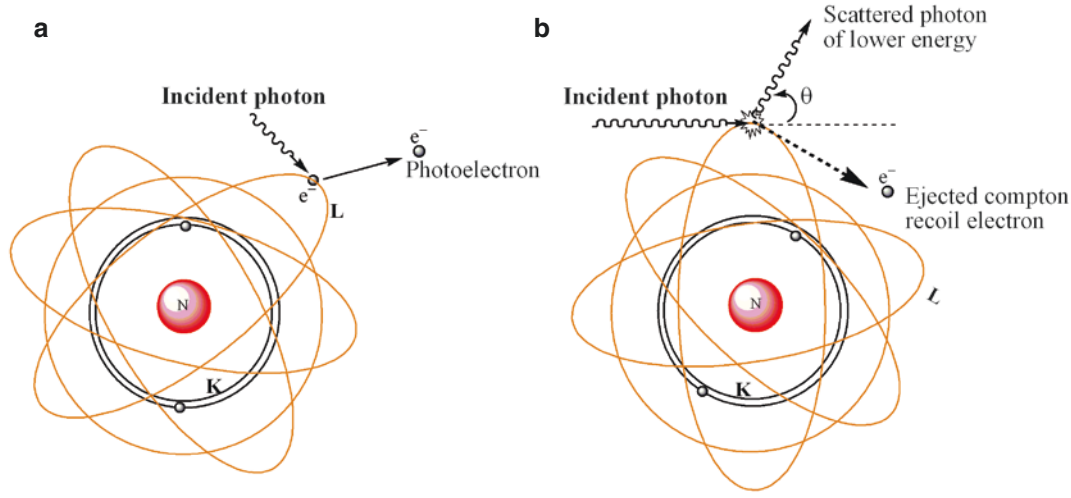

Fig. 5.2 Interaction of high-energy photons with matter. In the photoelectric effect (**a**), an incident photon transfers all its energy to an orbital electron, which leaves the atom and is known as a photoelectron. In Compton scattering (**b**), the incident photon transfers only part of its energy to an orbital electron, which is then ejected (recoil electron). The scattered photon is then deflected in a different angle (θ, the scattering angle)

photoelectric effect is usually accompanied by the emission of characteristic X-rays and/or Auger electrons.

The probability of a photoelectric interaction occurring at a particular shell depends on the energy of the incident photon and the binding energy of the shell (in other words, on Z). The probability is zero when the energy of the photon is less than the binding energy of the electron; it is greatest when the photon energy is equal to the binding energy of the electron and thereafter decreases rapidly with increasing photon energy. Following the injection of radiotracers, the photoelectric effect plays a minor role with soft tissue. In radiation detectors, such as scintillation detectors, however, the photoelectric effect is the predominant mode of interaction of photons.

5.1.2.2 Compton Scattering

Compton scattering is a collision between a photon and a loosely bound outer orbital electron. After the interaction, the *scattered photon* undergoes a change in direction and the recoil electron is ejected from the atom (Fig. 5.2). The scattered photon is deflected through an angle (θ_C) proportional to the amount of energy lost. The maximum energy loss occurs when the θ_C is 180° or when the photon is *backscattered*. For example, the annihilation photon (511 keV) after backscatter will have an energy of 170 keV. The energy lost by the scattered photon is divided between the small binding energy of the orbital electron and the kinetic energy of the recoil electron. The relative probability of Compton scattering increases slightly as the energy of the incident photon increases and as the effective atomic number (Z_{eff}) of the interacting medium decreases. Following administration of radiotracers, the most important and significant mode of interaction of photons with soft tissue is Compton scattering.

5.1.2.3 Pair Production

When a high-energy photon interacts with an electric field of a charged particle (atomic nucleus or even an electron), the incident photon may completely disappear and its energy is used to create a β^- and β^+ pair, known as *pair production*. Since the rest mass (energy) of the electron is 511 keV, the incident photon must have a minimum energy of 1.022 MeV. The difference between the incident photon energy and 1.022 MeV is imparted to the electron pair as kinetic energy.

5.1.3 Attenuation

If we measure the intensity of the radiation before (I_0) and after it interacts with a given medium (I_x) of particular thickness x, we find that the intensity of the radiation after passing through the medium has reduced; the beam of radiation is said to have been attenuated. By the processes of absorption and scattering in a medium, a beam of radiation undergoes attenuation. The atoms in the medium act as targets, which, if hit, will attenuate a photon from the primary radiation beam. The probability of an interaction with a particular atom is low, but the very large number of atoms in a small volume of a solid increases the probability of attenuation, significantly. A parallel beam of monoenergetic electromagnetic radiation will undergo exponential attenuation as it passes through a uniform medium.

$$I_x = I_0 e^{-\mu x} \tag{5.4}$$

where μ is the total *linear attenuation coefficient*, which can be defined as the fraction of photons removed from a beam of radiation per unit thickness of the attenuating medium. The parameter μ is a property of both the photon energy and the nature of the medium. It increases (i.e., photons become less penetrating) for low photon energies and low mass density. In a given thickness of medium, the number of atoms (N) may be the same for different materials, but the density (ρ) may vary. Therefore, the total mass attenuation coefficient μ/ρ is the fraction of photons removed from a beam of radiation of unit cross-sectional area by unit mass of the medium. For photons with <1 MeV energy, the parameters μ and μ/ρ are largely made up of components due to photoelectric absorption (τ) and Compton scattering (σ).

Other important parameters derived from m are half-value thickness (HVT) or half-value

Table 5.1 Linear attenuation coefficient and HVL values of photons for different materials

Material	Density (ρ) (g cm^{-3})	140-keV μ (cm^{-1})	Photon HVL	511-keV μ (cm^{-1})	Photon HVL
Water	1.0	0.15	4.62	0.095	7.29
Adipose tissue	0.95	0.142	4.88	0.090	7.70
Cortical bone	1.92	0.284	2.44	0.178	3.89
Pyrex glass	2.23	0.307	2.26	0.194	3.57
Lucite	1.19	0.173	4.01	0.112	6.19
NaI (Tl)	3.67	2.23	0.31	0.34	2.04
Bismuth germinate	7.13	~5.5		0.95	0.73
Lead	11.35	40.8	0.018	1.75	0.42
Tungsten				2.59	0.29

layer (HVL), tenth value layer (TVL), and the mean free path (MFP), which is the distance a photon (or a particle) travels before interacting. All these parameters are related mathematically as shown in the following equations:

$$\mu = 0.693 / \text{HVL} \tag{5.5}$$

$$\text{MFP} = 1.44\,\text{HVL} \tag{5.6}$$

With radiation, the three most important media of interest are the tissue, radiation detector material (the crystal), and the type of shielding (lead, tungsten). For various materials, the linear attenuation coefficient and HVL values for photons of two different energies, 140 and 511 keV, are shown in Table 5.1. For 511-keV photons, the primary interaction is Compton scattering; therefore, correction for attenuation and scattering is essential for PET imaging studies.

5.2 Radiation Detectors

Radiation detectors have been developed over the years on the basis of the two major consequences of interaction of radiation with matter: ionization and excitation. Radiation detectors are generally categorized as either ionization detectors or scintillation detectors.

5.2.1 Ionization Detectors

These detectors respond to radiation by means of ionization, which induces tiny electrical currents that can be detected and measured. The ionization detectors can be either gas-filled (also known as *ionization chambers*) or *semiconductor detectors*.

5.2.1.1 Gas-Filled Detectors

Most gas-filled detectors are made up of a chamber, which contains a volume of gas (mostly air or an inert gas) between two electrodes with a voltage difference between them. Under normal circumstances, the gas is an insulator and no current flows between the electrodes. When the gas is ionized following an interaction with radiation, electrons are attracted to the anode and positive ionized atoms are attracted to the cathode, producing a small current. When gas-filled chambers operate at the saturation voltage (300–600 V), to ensure complete collection of ions at the electrodes, they are called *ionization chambers*. If the detector is calibrated to express the measured current as an exposure rate (R h^{-1}, mR h^{-1}), it is called a survey meter; if it collects the total charge over a period of time, it is called a *pocket dosimeter*; and, finally, if the measured current is used to assay the activity (mCi, MBq, etc.), it is called a *dose calibrator*.

Ionization chambers are quite inefficient as detectors for X-rays and γ-rays. Their response to photons changes with photon energy, but the energy discrimination, especially in the case of dose calibrators, is achieved only by the use of precalibrated amplifiers, one for each radionuclide of interest.

If an ionization chamber is maintained between 900 and 1200 V, the electrons generated by the interaction of radiation will accelerate and cause additional ionization. This process is

known as *gas amplification* of the charge, and the factor by which the ionization is amplified is called the *gas amplification factor* (GAF). A Geiger–Muler (GM) counter is a gas-filled detector designed to have GAF as high as 10^{10}. In a GM counter, the size of the electrical signal output is relatively constant and independent of the energy of radiation. Because of their high sensitivity, GM counters are mainly used as survey meters to detect ambient radiation levels and radioactive contamination.

5.2.1.2 Semiconductor Detectors

Semiconductor detectors are essentially solid-state analogs of gas-filled detectors [1]. Semiconductor materials, such as Si and Ge, when doped with Li, can function as solid ionization chambers, and are also called *solid-state detectors*. In order to create an ion pair in air, the energy needed is 34 eV per ionization. In contrast, the energy needed to create an ion pair is only 2.5 eV in Si(Li) and 3.0 eV in Ge(Li) detectors. When a small voltage is applied across a semiconductor detector, a high-energy photon will interact with the detector and liberate electrons leaving a positive hole in the lattice structure. Under an applied electric field, both the electron and the positive hole will move toward opposite electrodes inducing an electric current. Since the size of the electrical signal is relatively large and proportional to the radiation energy absorbed, semiconductor detectors are useful for energy-selective radiation counting.

Both, Ge- and Si-based semiconductors conduct a significant amount of thermally induced electrical current at room temperature. Therefore, it is necessary to operate and maintain these detectors at relatively low temperatures. High-purity germanium (HPGe), however, needs to be cooled to low temperatures, while others such as cadmium telluride (CdTe) and cadmium zinc telluride (CZT) operate at room temperature. Ge(Li) and Si(Li) detectors are relatively inefficient for detecting high-energy gamma photons. Both, CdTe and CZT have stopping powers similar to NaI(Tl) scintillation detectors. Even denser semiconductors, such as lead iodide (PbI) and thallium bromide (TlBr), are currently under development and may be useful for detecting high-energy photons. CdTe and CZT are also available as pixelated detector arrays with a typical intrinsic spatial resolution of 2.4 mm.

5.2.2 Scintillation Detectors

When high-energy photons interact with the atoms of a scintillation crystal, the electrons are raised from a *valence band* or an orbital to a forbidden, unfilled *conduction band* of a higher energy state. The excited atoms quickly return to the ground state emitting a visible light in a process known as *luminescence*. The number of electrons raised to a higher energy level, and the consequent number of visible light photons emitted by the crystal, depends on the energy of the incident photon. The photoelectric effect is the primary mode of interaction of photons with the atoms in the crystal. The visible light emitted by the crystal is usually in the ultraviolet range. For the crystal to emit light in the visible range (400–500 nm), an alkali halide crystal, with an impurity of (<1%), such as thallium iodide, must be *activated* (or *doped*). The scintillation photons produced by the luminescence are emitted *isotropically* (in all directions) from the point of interaction. The most important scintillators used in PET and SPECT scanners are the following:

- Sodium iodide doped with thallium iodide (NaI(Tl))
- Bismuth germinate, $Bi_4Ge_3O_{12}$ (BGO)
- Lutetium oxyorthosilicate doped with cerium, Lu_2SiO_5:Ce (LSO)
- Yttrium oxyorthosilicate doped with cerium, Y_2SiO_5:Ce (YSO)
- Gadolinium oxyorthosilicate doped with cerium, Gd_2SiO_5:Ce (GSO)
- Barium fluoride (BaF_2)
- Lutetium yttrium oxyorthosilicate (LYSO)

The physical properties of several scintillators are compared in Table 5.2. The most important properties of a detector are stopping power, light output, signal decay time, and the intrinsic energy resolution of the crystal. The following points

Table 5.2 Physical properties of scintillators

	NaI (Tl)	YSO	BaF2	LYSO	GSO	BGO	LSO
Density (g cm^{-2})	3.67	4.53	4.89	5.31	6.71	7.13	7.4
Effective Z	50.6	34.2	52.2	54	58.6	74.2	65.5
Light output (photons/keV)	38	46	2	30	10	6	29
Relative light output (%)	100	118	5	76	25	15	75
Wavelength, λ (nm)	410	420	220	420	440	480	420
Decay time (ns)	230	70	0.6	53	60	300	40
Attenuation, μ (cm^{-1}) at 511 keV	0.3411	0.3875	0.4545	–	0.6978	0.9496	0.8586
Attenuation length ($1/\mu$)	2.93	2.58	2.20	2.0	1.433	1.053	1.169
Photoelectric/Compton ratio	0.22	–	0.24	–	0.35	0.78	0.52

may be noted: (1) The stopping power is characterized by the MFP or attenuation length, which depends on the density (ρ) and effective atomic number (Z_{eff}) of the crystal. A crystal with shorter attenuation length will have higher efficiency and sensitivity. (2) A crystal with high light output (photons keV^{-1} absorbed) will have good energy resolution. (3) A short decay time of the crystal can help process each pulse separately at higher counting rates with minimum dead time. (4) A crystal with better energy resolution can reject scattered photons more effectively. The overall scanner spatial resolution, however, depends on several other factors.

With NaI(Tl) crystal, the detection efficiency for 140-keV photons is >90%, but for 511-keV photons, the efficiency drops to <10%. The intrinsic energy resolution of the crystal is more important for SPECT scanners, while the stopping power of the crystal is one of the main considerations in the choice of the crystal that can interact with 511-keV photons in PET scanners. With the current PET scanners, BGO and LSO are the preferred crystals, while NaI(Tl) is the only crystal that is used in all the major clinical SPECT scanners. A number of other scintillators such as CsI(Tl) and CsI(na) are also under evaluation. The technology of PET and SPECT scanners is continuously evolving and is dependent on many other factors besides scintillators.

5.2.2.1 Photodetectors

One of the common characteristics of all scintillators is that following interaction with high-energy photons they all produce a very weak signal of visible light, or a scintillation photon. The purpose of a photodetector is to convert a scintillation photon with 3–4 eV energy into an electrical current. The probability of converting a photon into an electron is called *quantum efficiency*. The two categories of photodetectors used are photomultiplier tubes (PMTs) and semiconductor-based photodiodes.

A PMT is a vacuum tube that consists of an entrance window, *photocathode*, followed by a series of *dynodes* (electrodes), each of which is held at a greater voltage with a resistor chain. The scintillation photon strikes the photocathode and release photoelectrons, which are then accelerated to the first dynode and release even more electrons, which are then accelerated to the next dynode. After passing a series of dynodes, the number of electrons is amplified to $>10^6$, producing a sizeable current in the milliampere range at the anode. Despite their bulkiness, almost all commercial PET and SPECT scanners use PMTs because of their high gain or amplification, ruggedness, and stability. The quantum efficiency of the photocathode in PMTs is about 15–25%. In order to improve this efficiency, more advanced PMTs, known as position-sensitive (PS) PMTs and multichannel (MC) PMTs, are under development and evaluation.

A photodiode consists of a thin piece of doped silicon wafer (a couple of 100 μm thick). The principle of operation is the same as that of a semiconductor. The quantum efficiency (60–80%) of photodiodes is much better than that of PMTs, but the signal of the electrical current is very weak because photodiodes do not have internal amplification or gain. In order to improve the signal-to-noise ratio (SNR), a new type of

photodiode known as *avalanche photodiode* (APD) has been developed, which has an internal amplification; however, it is still not as good as that of PMTs.

5.2.2.2 Radiation Detector Performance

Spectroscopy is the study of the energy distribution of a radiation field. Most spectrometers are operated in the pulse mode and the amplitude of each pulse is proportional to the energy deposited by the interaction of the photon with the crystal. The amplitude, however, may not be proportional to the total energy of the incident photon. A *pulse height spectrum* (Figs. 5.3 and 5.4) represents the number of interactions or counts per minute (cpm) as a function of the energy of the photon, but it is not the same as the actual energy spectrum of the incident radiation. The performance characteristics of radiation detectors can be expressed quantitatively using parameters, such as *sensitivity* and *energy resolution*.

Sensitivity (or *efficiency*) is the detected count rate per unit of radioactivity. *Geometric sensitivity* of a detector is the fraction of emitted photons that reach the detector, whereas the *intrinsic sensitivity* or the *quantum detection efficiency* (QDE) is the fraction of those photons that reach the detector which are actually detected. For example, 1 μCi of ^{99m}T has 2.2×10^6 disintegrations per minute (dpm), and each decaying atom produces one 140-keV photon. If the detector can detect 1.0×10^5 photons, then the sensitivity of the detector is 10%. As discussed previously, various physical characteristics of the crystal (Table 5.2) can affect the sensitivity of the scintillator.

Many radionuclides emit a number of photons (X-rays and γ-rays) of discrete energies. The electrical signal output from a detector–photodiode combination, however, appears as though it is coming from a range of energies due to the absorption and scattering of the incident photons. Energy resolution quantifies the ability of a specific crystal to differentiate or discriminate photons of different energies. It is expressed quantitatively as a percent of full width at half-maximum (FWHM = ΔE) of an energy spectrum (counts detected vs. energy (keV)) of a radionuclide with a specific photopeak energy (E_γ).

$$\text{FWHM}(\%) = \frac{\Delta E}{E_\gamma} \times 100 \tag{5.7}$$

For energy-selective detection (as in Anger cameras), the FWHM determines the resolution of the detector. The sensitivity can be increased by increasing the value of ΔE, but that would degrade the resolution.

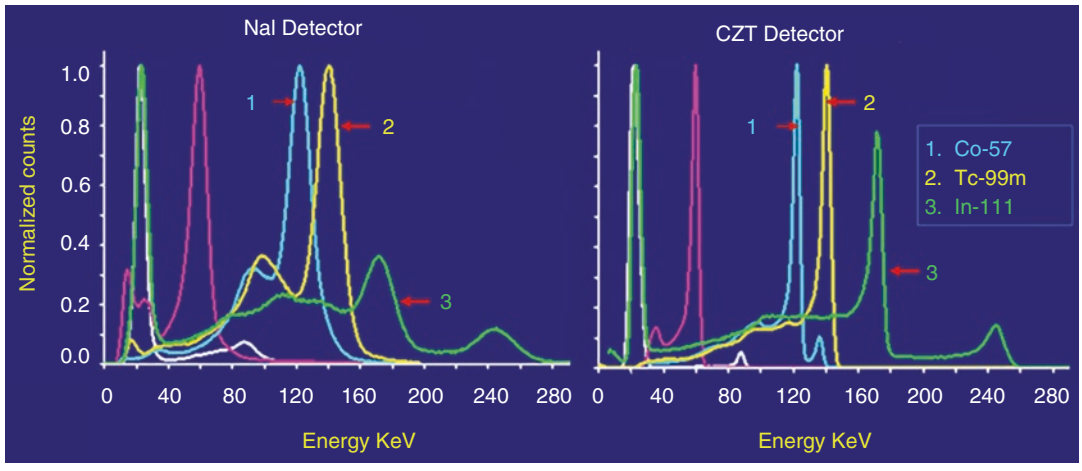

Fig. 5.3 Pulse height spectra of several radionuclides using NaI or CZT detector. The energy resolution with CZT detectors is much higher compared to that with NaI detector

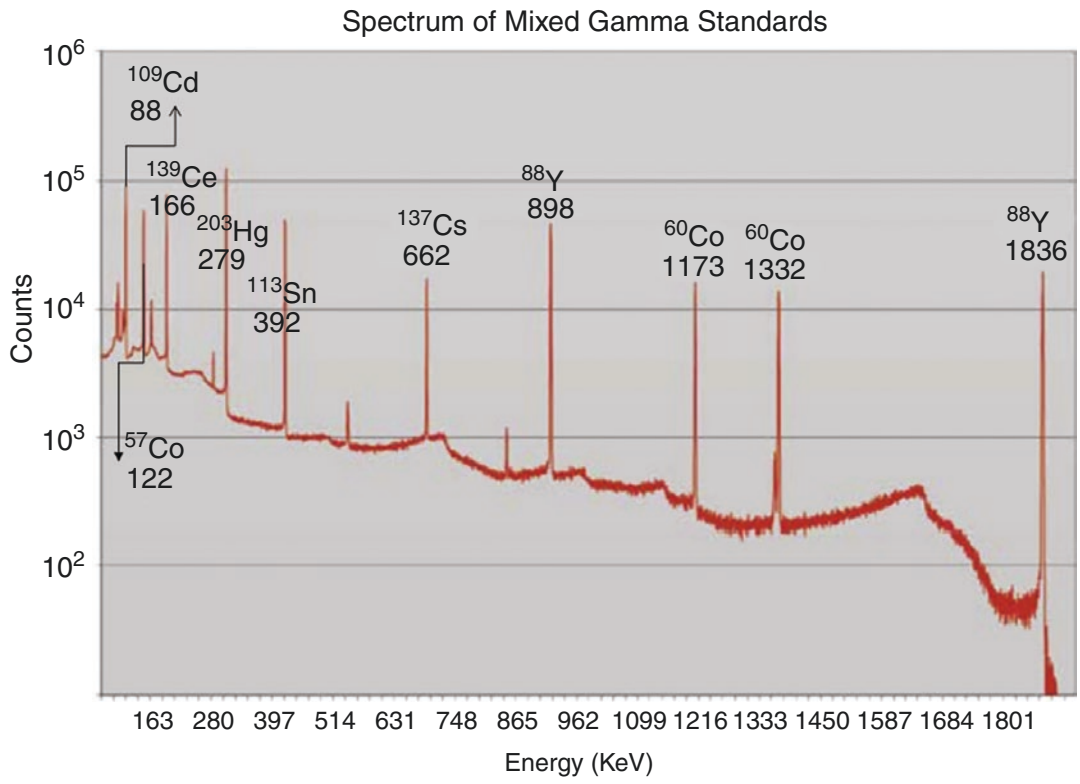

Fig. 5.4 Gamma spectrum of Analytics mixed standard using high-purity germanium (HPGe) detector. Analytic's mixed gamma standard utilizes the basic eight radionuclides which show minimal spectral interference

5.3 Radionuclide Imaging Systems

The purpose of radionuclide imaging is to obtain an image of the in vivo distribution of a radiotracer on the basis of the external detection of high-energy photons emitted by the radionuclide. In the 1940s, attempts were made to detect the distribution of radioactivity in vivo, but it was only in the 1950s, that in vivo radionuclide imaging became a practical clinical modality, due to the introduction of the rectilinear scanner, by Ben Cassen. In the 1950s, Hal Anger developed the first γ-ray camera using a single, large-area NaI(Tl) scintillation crystal coupled to PMTs. This camera, subsequently, called the *Anger scintillation camera*, has become the predominant molecular imaging device in nuclear medicine. Since then, many refinements and modifications have been made to improve the image quality of this camera.

Conventional Anger camera images compress the three-dimensional (3D) distribution of the radiotracer into a two-dimensional (2D) image. As a result, the contrast between areas of interest and the surrounding territory is often significantly reduced. In *planar imaging* systems, the radiation from a source (patient) is collected and the data are presented as though all photons are coming from a single plane. In a patient, images of a specific area of interest at one depth are obscured by images of structures above and below the area of interest. *Tomography* simply means an image of a slice. Tomographic images are 2D representations of structures lying within a selected plane or depth in a 3D object. *Computed tomography* (CT) techniques are based on rigorous mathematical algorithms initially developed by Radon, in 1917. The introduction of CT, in the 1970s, helped to implement CT techniques to the radionuclide imaging methods. X-ray CT is a transmission CT since X-rays from an external

source are transmitted through the patient to a detector. With radiotracers, high-energy photons are emitted from the patient; this technique is called *emission computed tomography* (ECT). While single photon emission computed tomography (SPECT) is based on radionuclides (such as ^{99m}Tc, ^{123}I, and ^{111}In) that directly emit single high-energy photons, positron emission tomography (PET) is based on positron-emitting radionuclides, and detection of high-energy (511 keV) photon pairs resulting from an annihilation process of positrons and electrons. The detection concepts used in the PET scanners make PET about 10–100 times more sensitive than SPECT and at the same time provide clinical PET images with higher spatial resolution.

PET and SPECT provide functional images of radiotracer distribution. In order to localize the tracer distribution, PET and SPECT are usually combined with structural imaging modalities that offer anatomical information with high spatial resolution, such as computed tomography (CT) and magnetic resonance imaging (MRI). These so-called hybrid-imaging modalities, PET/CT, PET/MRI, and SPECT/CT nowadays are standard in most nuclear medicine facilities. Also, CT and MRI are also used to improve the quantification of PET and SPECT. Several reviews described the technical developments of the hybrid scanners in greater detail [2–6].

5.3.1 SPECT/CT Scanner

Functional nuclear medicine imaging with SPECT/CT has been commercially available since the beginning of this century. Most of the SPECT systems available are based on the well-known Anger camera principle with NaI(Tl) as a scintillation material, parallel-hole collimators, and multiple photomultiplier tubes, which, from the centroid of the scintillation light, determine the position of an event. Recently, solid-state detectors using cadmium–zinc–telluride (CZT) became available and clinical SPECT cameras employing multiple pinhole collimators have been developed and introduced in the market. Quantitative studies with SPECT are still work in progress; however, significant improvements have been made with CZT-based SPECT scanners. Most commercial SPECT/CT systems with dual-head or ring detectors (Fig 5.5), offered by General Electric (GE) Healthcare, Siemens Medical Solutions, Philips Healthcare, and Mediso Medical Systems all offer high-resolution diagnostic CT units as part of their SPECT/CT systems. Mediso even offers a complete SPECT/CT/PET with high-resolution LYSO detector technology as part of their AnyScan family of systems [2].

5.3.1.1 SPECT Based on NaI(Tl) Crystal

The principles of SPECT imaging with the commonly used scintillation camera based on the Anger camera design [7] consists of a single rectangular NaI(Tl) crystal (~50–60 cm in area) optically coupled to a large number of PMTs (typically 37–91). While the thickness may vary from 0.25 in. (~6 mm) to 1 in. (~25 mm), most cameras are made up of a 3/8 in. (~10 mm) crystal for optimum performance of radionuclides with energies between 120- and 200-keV photons. A *collimator* (usually made of lead) with holes (round, square, rectangular, or hexagonal) allows high-energy photons coming from the patient in a specific direction to enter and interact with the crystal. The walls, called *septa*, around the holes in the collimator absorb photons (~99% of photons reaching the collimator) that are traveling in an oblique angle to the axes of the holes. In other words, the collimator controls the direction of the photons entering the crystal. The thickness of the collimator and septa as well as the number of holes determines the overall sensitivity and resolution of the Anger camera. Most cameras have a wide choice of parallel-hole collimators such as "low-energy high sensitivity," "low-energy all purpose (LEAP)," "low-energy high resolution," medium-energy, high-energy, and ultrahigh-energy collimators, each designed to optimize a specific imaging study. With all parallel-hole collimators, the spatial resolution degrades rapidly as the distance (space) between the patient and the collimator increases. A pinhole collimator consists of a small hole (3–5 mm in diameter) in a piece of lead or tungsten and is

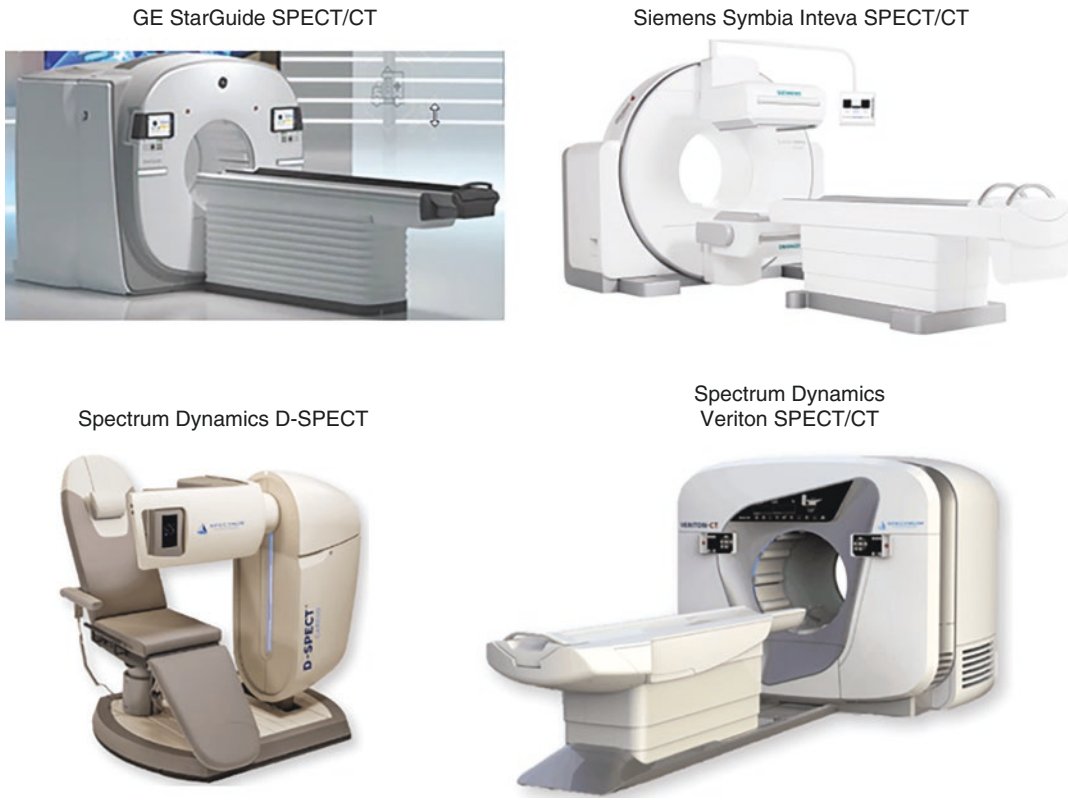

Fig. 5.5 SPECT/CT systems in routine clinical use. GE Healthcare StarGuide, the most advanced SPECT/CT featuring advanced Cadmium Zinc Telluride (CZT) technology. Spectrum Dynamics CZT based digital systems include D-SPECT for cardiac applications and Veriton series for 360° total-body digital SPECT/CT. Siemens Healthineers Symbia Intevo dual-head SPECT/CT with high sensitivity

commonly used to produce magnified views of small objects. The magnification and sensitivity, however, decrease as an object is moved away from the pinhole. Following interaction of photons with the crystal, the emitted light photons induce electrical signals in the PMTs. In a NaI(Tl) crystal, approximately one visible photon is emitted for every 25 eV of energy deposited. For example, when a 140-keV photon deposits all of its energy in the crystal, it will generate 5600 visible light photons, of which only 20–25% may eject electrons from the photocathode and contribute to the signal from the PMT. The PMTs closest to the scintillation even in the crystal receive more light than those that are most distant and as a result produce a larger electrical signal. The relative amplitude of these pulses determines the location of the interaction in the crystal and the exact location of the origin of the photons coming from the patient. The electrical pulses from PMTs pass through preamplifiers and ADCs (analog-to-digital converter). The digital *X*, *Y*, and *Z* signals are corrected using correction circuits, followed by energy discrimination using SCAs (single-channel analyzers). The signals are finally converted into digital images in a computer. The measures of performance of a scintillation detector or camera alone are called *intrinsic* measurements, while the measures with the collimator are called *extrinsic* or system measurements; these measurements give the best indication or clinical performance.

With many of the Anger scintillation cameras, the intrinsic spatial resolution (R_i) for 140-keV photons of ^{99m}Tc is between 2.7 and 4.0 mm. With a parallel-hole collimator, however, the sys-

tem resolution (R_s) could dramatically decrease to 8–12 mm at a distance of 10–20 cm from the collimator surface. Also, the system resolution is not the same in the entire field of view.

5.3.1.2 SPECT Based on CZT Detector

Unlike the original SPECT technology based on Anger gamma camera, which relied on the pairing of scintillators to photomultiplier tubes, the commercial SPECT systems based on cadmium–zinc–telluride (CdZnTe or simply CZT) were introduced more than a decade ago [8, 9].

CZT is a semiconductor-based solid-state detector material with a density of 5.78 g cm^{-3} that generates signals from the collection of induced charge created by the ionizations from photoelectric interactions or Compton scattering. When the photons interact with the CZT in the semiconductor, the incident γ-rays create electron pairs, and an electrical signal is produced. The direct conversion of energy in the CZT detectors is characterized by good energy resolution (Fig. 5.3), and in clinical applications, the energy resolution is reported to be better than 6% at 140 keV. Unlike other detectors (e.g., germanium), CZT operates at room temperature due to the large size of the band gap in the CZT detector [10]. The high atomic number of CZT assists in efficient photoelectric absorption, leading to an improved system sensitivity compared with that of the sodium iodine (NaI) detector [11]. The major advantages of these new CZT modules are the small size of the CZT module and the absence of PMTs, which allows for a compact camera but still with multiple detectors. This means that it is possible to increase the overall system sensitivity significantly as compared with traditional SPECT systems. The improvement in sensitivity can be used to reduce the acquisition time of a given administered activity or decrease the amount of radioactivity dose injected.

The first clinical system, introduced in the market, was the D-SPECT (Spectrum Dynamics, Caesarea, Israel) and this was followed later by the Discovery NM 530c (GE Healthcare, Haifa, Israel). Both systems have a C-shaped gantry that contains multiple detectors. The number of detectors is, however, different between the systems. The GE Discovery NM 530c has 19 stationary detectors equipped with pinhole collimators while the D-SPECT has ten CZT detectors where each is equipped with a parallel-hole square hole collimator, made of tungsten, and where each detector swivels around its own axis to acquire an optimized number of projection angles. The advantage of these SPECT scanners is the ability to perform fast dynamic SPECT with both these systems since all projections are acquired simultaneously. The first clinical CZT devices that were introduced were anatomically specific for cardiac examinations [12]. However, the general-purpose device continues to have the well-known design with a gantry and multiple detector heads. The first example of a general-purpose CZT device, coupled with a CT, was introduced by GE Healthcare (NM/CT 870 CZT DIGITAL SPECT/CT). Several clinical studies using this device have been reported, covering different aspects including the reduced radiation burden due to higher sensitivity, verification of dual-radionuclide imaging, and short time acquisition using Tc-99m and I-123 in myocardial blood flow tests [13]. Spectrum Dynamics (Shanghai, China) and GE Healthcare presented a different approach with their Veriton and StarGuide systems, respectively. While conventional SPECT devices have detector heads attached to a rotating gantry, and their tomography image acquisition is obtained by positioning the heads at different angles, the ring-shaped SPECT uses the same design as PET. The detectors are positioned in fixed positions (12 dedicated positions for both devices) around the ring, and the acquisition is obtained using these fixed positions.

5.3.1.3 Absolute Quantitation of SPECT Data

A major image-degrading process in SPECT is the scatter and resultant attenuation of photons as they traverse through the tissue before they reach the detector. Reliable attenuation and scatter compensation (ASC) is a pre-requisite for quantification tasks, such as quantifying biomarkers from SPECT images or performing SPECT-based dosimetry. Methods for absolute quantitation of SPECT images provide an estimate of the

activity uptakes in various organs and tissues in units of mBq or mCi/mL. Clinically valid semi-quantitative measure is the standard uptake value (SUV), also known as standardized uptake value or the dose uptake ratio (DUR). As the name suggests, it is a mathematically derived ratio of tissue radioactivity concentration at a point in time $C(T)$ and the injected dose of radioactivity per kilogram of the patient's body weight [14]. Because SPECT images generally are hampered by several physical and camera-specific effects, accurate and precise compensation methods are required. The most important effects such as photon attenuation in the patient, contribution of events from photons scattered in the patient and the collimator but accepted by the energy window, the effect of the collimator response function that degrades the image quality because of the relatively poor spatial resolution. All these effects can reduce the accuracy and precision in the activity concentration estimate. In addition to these compensation methods, a careful and consistent calibration is needed to translate counts in the image that corresponds to a location in the patent to activity, or activity concentration [3]. Based on xSPECT Quant™ technology and Symbia Intevo SPECT CT (Siemens Healthineers), the potential utility of quantitative SPECT was evaluated by the determination of standard uptake values (SUV_{max} and SUV_{mean}) with several SPECT radiopharmaceuticals [15]. While the results do show some clinical value, absolute quantitation in SPECT is still work in progress. In combination with iterative reconstruction methods with proper modeling of photon attenuation, scatter and collimator resolution degradation, SPECT/CT systems will be very useful for studies requiring patient-specific dosimetry or dose planning and longitudinal studies, especially when longer half-life radionuclides such as ^{89}Zr may not be ideal to develop targeted radiopharmaceuticals for PET.

5.3.2 PET Scanners

PET scanners were designed to obtain in vivo images of the distribution and uptake of radiotracers on the basis of β^+ emitting radionuclides, and the ability to detect, and localize the positron-emitting nuclei by using coincidence counting to capture the paired annihilation of high-energy photons (511 keV) emitted following positron annihilation with an electron. The sensitivity of PET is the ability to detect low molecular mass of the radiopharmaceutical, which depends on the ability of the radiochemistry to produce labeled compounds with high specific activity (GBq or mCi/μmol). The power of the technique lies in the availability of more PET radionuclides than SPECT radionuclides and the wide range of available radiotracers that produce image contrast directly related to underlying physiology, metabolic pathways, or molecular targets. Using today's advanced PET scanners, radiotracers can readily be detected at trace mass levels (nanomolar concentrations or less) and using a dynamic sequence of images and the principles of tracer kinetic modeling, parameters related to the transport, metabolism, or binding of the tracer can be quantitatively derived [16].

One of the first positron imaging devices, the *positron camera* was developed in 1969 by Dr. Brownell and his team at Massachusetts General Hospital (MGH) in Boston [17]. That device consisted of only two planar arrays of crystals. Over the course of the last 50 years, coincidence detection of positron-emitting radionuclides has evolved from single pairs of detectors for planar imaging to current PET scanners with arrays of detector elements covering typically 25 cm or more, in axial length that contain on the order of 35,000 individual detector elements. Currently, the first total-body PET scanner, the EXPLORER, is which is 2 m in axial length and contains 560,000 individual detector elements [18, 19]. Developments have centered on improvements in the scintillator crystal and photodetector combination, the acquisition electronics and advances in data processing, reconstruction, and image analysis. Moreover, the introduction of digital PET offers the possibility to reduce radiation dose and scan times which may facilitate the implementation of PET to address unmet clinical needs [20]. In the last two decades, PET was successfully integrated, in 2000, with CT and subse-

quently with MRI, to create powerful hybrid-imaging systems that can interrogate structure, and function in the same imaging examination.

A typical PET scanner consists of many rings of scintillation detectors which surround the subject. The PET scanner uses the *annihilation coincidence detection* (ACD) method to obtain projection images of the radiotracer distribution. The images are first corrected for attenuation, scatter, etc., and then mathematically processed, as in the case of CT and SPECT, to obtain transverse images of several slices of the body in a given field of view (FOV). A number of reviews have been published, describing the historical development of the PET technology [16, 19–22].

5.3.2.1 Positron Annihilation and Coincidence Detection

A positron ejected by a radionuclide travels a very short distance in a tissue, dissipating its kinetic energy in collisions with electrons, and finally combines with an electron to form a positronium, a state which lasts for a very short time (10^{-10} s). The subsequent positron–electron annihilation results in the emission of two 511-keV photons, 180° apart. A PET scanner is designed to detect this pair of annihilation photons almost simultaneously on the basis of a process known as ACD, which establishes the trajectories of detected photons or lines of response (LOR). ACD only establishes the location of an annihilation event within the LOR; the exact location of a positron-emitting radionuclide, however, is determined mostly using the CT techniques, based on mathematical processing of millions of LOR to generate a computed tomogram of the PET tracer distribution. In a different approach, known as *time-of-flight* (TOF) method, measuring the difference in arrival time of the two annihilation photons at the opposite detectors helps to determine the exact location d of the annihilation event along the LOR.

Positron Range and Noncolinearity

Determining the exact LOR along which a positron-emitting radionuclide can be found is one of the major factors that determine the spatial resolution of a PET scanner. *Positron range* and *noncolinearity* are two effects that may lead to errors in determining the LOR.

Positron-emitting radionuclides differ in the kinetic energy of the emitted positrons. For example, the energy of positrons emitted by ^{18}F (E_{max} = 0.63 MeV) is almost one-fifth that of a positron emitted by ^{62}Cu (E_{max} = 2.93 MeV). The positron range (is similar to the beta particle range in tissue) is the direct distance traveled by the positron from the decaying atom to the exact location of the annihilation event. The positron range is a function of the kinetic energy of the positron (Fig. 5.6). The mean positron range may vary from a fraction of a millimeter to 4–6 mm, depending on the radionuclide. The error due to the positron range may be significant and, therefore, this range limits the ultimate resolution attainable by PET. It is very important to appreciate the fact that the SPECT technique inherently offers no limitation in spatial resolution due to photon energy, while the PET technique has a theoretical limit in terms of spatial resolution.

In contrast to the positron range, noncolinearity is independent of the positron-emitting radionuclide. The positron and electron are not exactly at rest when the annihilation occurs. As a result, the two annihilation photons differ in their momentum and are not emitted exactly at 180°

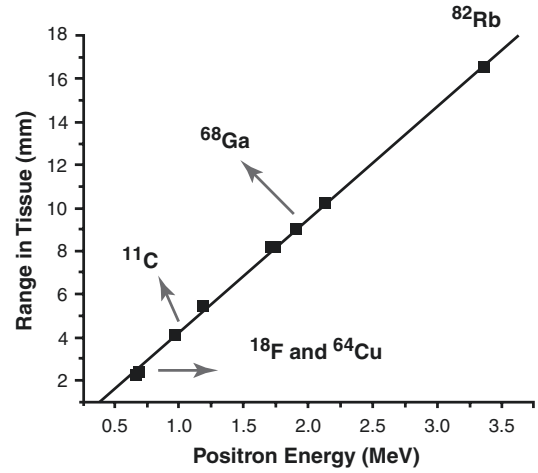

Fig. 5.6 The positron range in tissue as a function of positron energy

apart (they may be emitted with a distribution of angles around 180° (typically ±0.25°)). For a given PET scanner with diameter D, this blurring effect, due to noncolinearity (Δ_{nc}), can be estimated as follows:

$$\Delta_{nc} = 0.0022 \times D(\text{in mm}) \qquad (5.8)$$

With most clinical PET/scanners that have a ring diameter of ~80 cm, the blurring due to a noncolinearity error may be 1.76 mm. However, in MicroPET, this effect is somewhat less significant.

Coincidence Event Types

A *true coincidence* is the simultaneous interaction of a pair of photons (511 keV) resulting from the annihilation of a positron-electron pair (Fig. 5.7). A *random coincidence* occurs when two 511-keV photons from separate annihilation events, that occurred as a result of the decay of different atoms, strike the opposite detectors, simultaneously. In the tissue, the 511-keV photons undergo scatter and lose some energy. A *scatter coincidence* occurs when one or both of the 511-keV photons from a single annihilation event are scattered but, simultaneously detected, by the opposite detectors. The total number of events (true, random, and scatter) detected by the coincidence circuit in a PET scanner is referred to as *prompt coincidences*. Also, when 511-keV photons or the scattered photons are detected, they are referred to as "singles." Since photons travel at the speed of light (30 cm ns^{-1}), the detection times of a pair of photons by the coincidence circuit can be between 2 and 3 ns. Typically, a coincidence timing window (τ) of 6–12 ns is used to account for statistical fluctuations in timing the detection events.

5.3.2.2 Pet Scanner Design

Since the early 1970s, several different PET detector configurations have been developed. In most dedicated PET scanners, pixilated or multicrystal detectors are arranged in rings or polygonal arrays completely encircling the patient. In addition, two or three planar large-area detectors (as in Anger camera) are also used to configure the PET scanner. The majority of current clinical PET and MicroPET scanners, however, are based on the full-ring configuration (Fig. 5.8). Scintillation crystals coupled to PMTs are used as detectors. Compared to full-ring detectors, the efficiency of other detector configurations for coincidence detection is significantly poor (<30%). A PET scanner typically consists of several components:

- Detector consisting of a scintillator coupled to PMTs
- Collimator

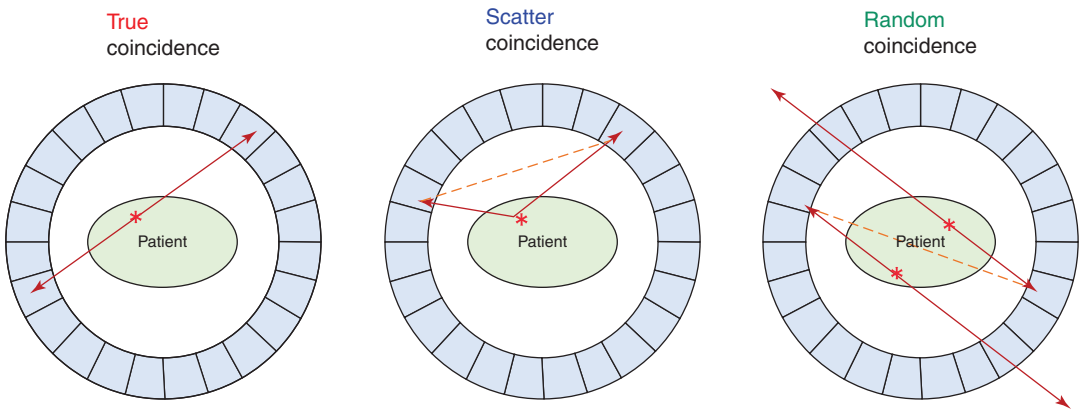

Fig. 5.7 In a PET scanner, the 511 keV photons from the patients are detected by coincidence counting. True counts are due to one annihilation and the photon path is straight in opposite directions. In random coincidence, photons from different annihilations will be detected, simultaneously. Scatter counts represent detection of scatter photons, simultaneously

Fig. 5.8 The typical PET scanner with ring detector configuration

- Signal processing electronics
- Coincidence circuit
- Data acquisition computer
- Reconstruction, display, and image analysis systems

The basic principles of a PET detector and collimation are discussed below. The electronics associated with the signal processing and the computer hardware needed for data acquisition, image processing, etc. are highly technical, and are discussed in detail in many other publications [21, 23, 24].

PET Detector Crystals

There are several ways in which the choice of PET scintillating detector material affects image quality [5]. The denser the material, the higher its photoelectric fraction, or its ability to stop the incoming 511-keV radiation completely on the

first interaction. Also, high luminosity or light yield (expressed as the number of light photons emitted for each MeV of energy absorbed) is desirable for signal-to-noise considerations. Finally, the speed at which a detector emits light after absorbing a 511-keV γ-ray is directly proportional to its count rate capability, which is important in 3D acquisitions. The decay time is defined as the time needed for the detector's light output pulse to decrease to 36.7% of its maximum-amplitude value and a low decay time is virtually essential for TOF imaging. Table 5.2 shows the characteristics of several PET scintillator materials, such as BGO, LSO, and LYSO. Most commercial PET scanners use detectors, typically 18- to 25-mm-thick crystals of LYSO or BGO scintillators that result in detection efficiencies of 80–90%, and time-of-flight capabilities of ~400 ps or better with lutetium-based scintillators [16].

Block Detector

In early PET scanners, each scintillation crystal was coupled to a single PMT and the size of the crystal largely determined the spatial resolution of the PET scanner. Smaller crystals were needed to improve the resolution. Since the size of PMT is relatively large, it was difficult to couple one PMT for each of the small crystals. In the 1980s, a multicrystal, two-dimensional BGO *block detector* system was developed [21]. The majority of dedicated clinical PET scanners in use today are based on the block detector design. A schematic of the block detector is shown in Fig. 5.9.

A block of scintillation detectors is made by segmenting (cutting or channeling) a relatively large block of crystal. The size of the individual elements in a matrix (block) PET detector ranges from $4 \times 4 \times 20$ mm^3 of LSO to $6.3 \times 6.3 \times 30$ mm^3 of BGO [5]. The channels are filled with a light-reflective material to prevent conduction of light from each crystal element to the next in the block. The scintillator block is then coupled to four PMTs and requires a high voltage (1600–1800 V) supply. Most PET scanners consist of 144–288 block detectors and contain 10,000–20,000 detector elements. With block detectors, Anger logic must be employed to estimate the location of the photon's original impact, limiting further improvement of spatial resolution in PET imaging. Although this still allows for high spatial resolution of 4–5 mm at the center of the field of view (FOV), great improvements have been achieved in the way detectors interface with the scanner's front-end electronics [5].

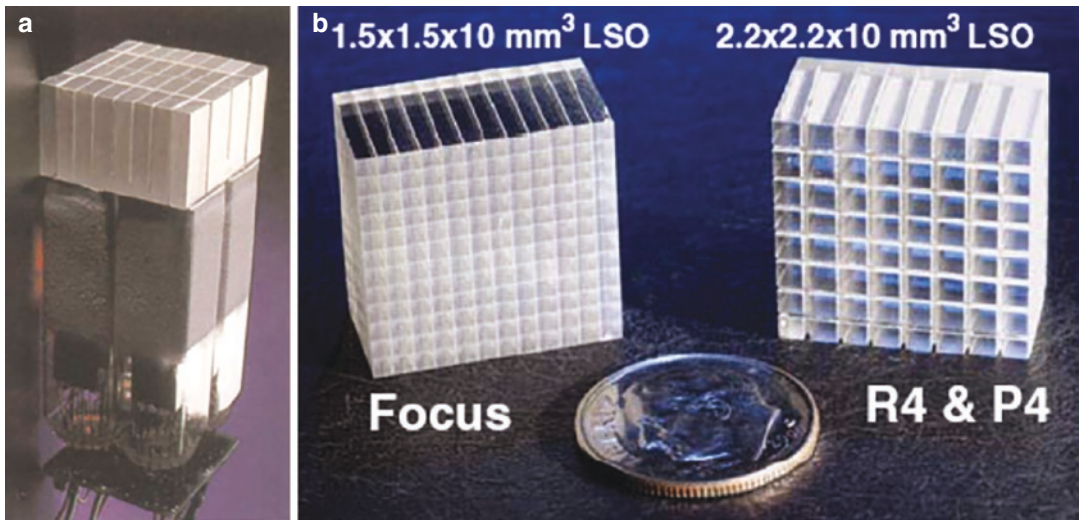

Fig. 5.9 The "block" detector (**a**), and Crystal arrays (**b**) used in the construction of MicroPET scanners [25]

Digital PET

Recent PET scanner designs feature smaller silicon digital photomultipliers (SiPM) or avalanche photodiodes [26]. The introduction of SiPMs as an alternative to standard PMTs used in analog PET scanners with block detectors. SiPMs, the basis for the so-called digital PET/CT systems, are smaller than standard PMTs (enabling higher spatial resolution) and provide up to 100% coverage of the crystal area, as well as high sensitivity, low noise, and fast timing resolution. Also, SiPMs in combination with optimized acquisition and reconstruction parameters improve the localization of the annihilation events, provide high-definition PET images, and offer higher sensitivity, and higher diagnostic performance [20]. This novel technology is actually used in different PET devices manufactured by different vendors, including Philips Healthcare (Vereos PET/CT), GE Healthcare (Discovery MI PET/CT), and Siemens Healthineers (Biograph Vision PET/CT system). The design of the digital system of different vendors, however, may have variations in the number of detector modules and the size of crystals. In principle, since each scintillation crystal is coupled to a single SiPM (1:1 coupling), there is an enhancement of the TOF and a reduction of the dead time, as well as an improvement in spatial, and timing resolution. Based on many clinical studies, it was concluded that Digital PET opens new perspectives in the quantification and characterization of small lesions, which are mostly undetectable using analog PET systems, potentially changing patient management, and improving outcomes in oncological, and nononcological diseases [20].

5.3.2.3 PET Data Acquisition

In order to obtain PET images of a radiotracer distribution, the data acquisition involves obtaining two different scans; a transmission and emission scan, while the patient is in the scanner. In addition, two other scans, called *blank scan* and *normalization scan*, are necessary to process, and reformat the PET projection data into a quantitative PET scan, with multiple slices.

Attenuation Correction Based on CT

Attenuation correction (AC) for the 511 keV photons originating from different parts of the body has been used in PET imaging ever since the introduction of the first PET scanners but, was originally based on radionuclide transmission rod sources circling around the patient to collect photon attenuation maps. With older PET scanners and several MicroPET devices, a transmission scan is first obtained by using external rod sources of radiation. The most common rod source is based on long-lived ^{68}Ge ($T_{½} = 270$ days), which decays by EC to ^{68}Ga, which in turn, decays by positron emission.

With the current PET/CT scanners, the most common method for attenuation correction is based on the CT scan. The maximum number of detector rows for the CT scanner component of a PET/CT is 128 although a CT scanner of 16 detector rows may be adequate for most clinical studies. A nondiagnostic CT scan can be used as a transmission scan. Since the CT scan is based on lower energy (~60-keV) X-ray photons, the CT scan can be performed either before or after the administration of a PET radiotracer. In addition, a CT scan for attenuation correction takes only 0.5–2 min.

A blank scan (with no object in the FOV) must be completely noise free and is generally performed for 1 h or, at least 10 times the duration for which the emission scan is obtained. The blank scan is obtained using a rod source or CT scan depending on the technique used for the attenuation correction (Fig. 5.10).

2D vs. 3D PET

There are two kinds of collimation used in PET: one to direct the photons to the detector and the other to select the detected events. Thick lead rings are used to define the external axial FOV, while thin lead or tungsten rings (1–5 mm thick) (usually referred to as septa) are employed to define the individual imaging planes. These septa can be positioned to define the slices during 2D PET studies, but can be retracted during 3D PET acquisition, to increase sensitivity.

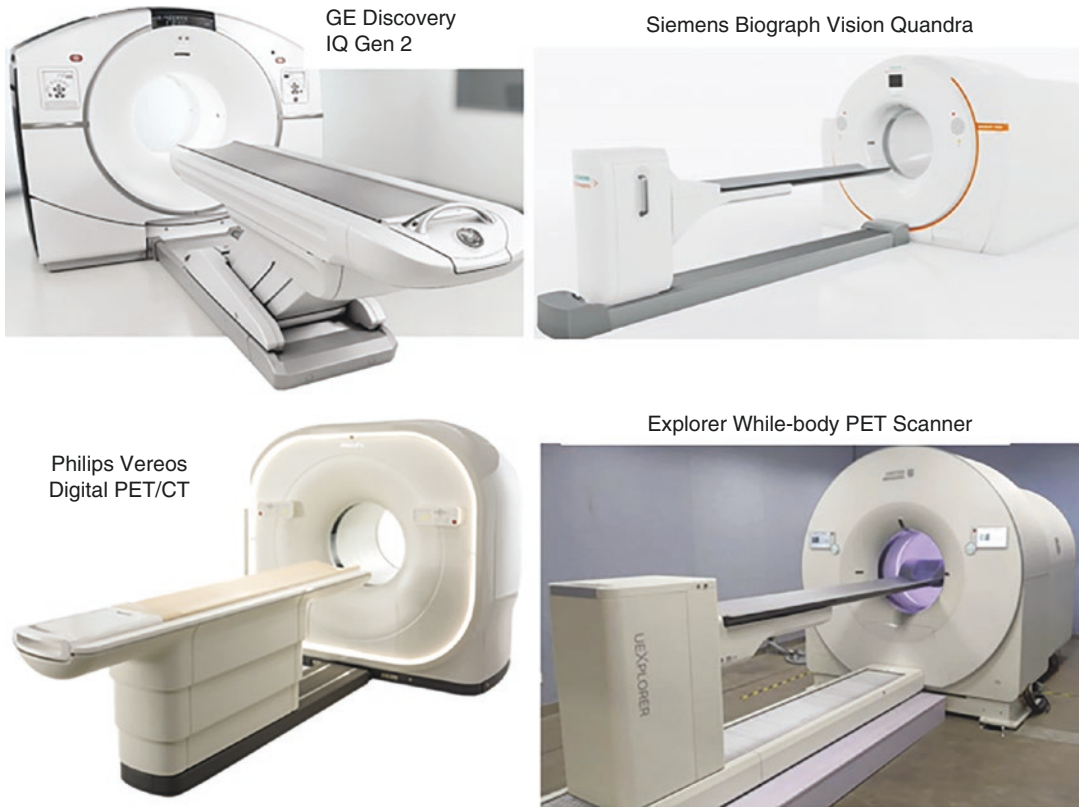

Fig. 5.10 PET/CT scanners: GE Discovery IQ Gen 2 is the next generation of our high-performance PET/CT system with faster scan times, with Motion-Free image clarity. Siemens Biograph Vision Quandra has a large axial PET field of view. To cover dynamically from vertex to thighs, Philips Vereos is the world's first and only fully digital, clinically proven, PET/CT scanner. The Explorer whole body PET scanner was developed by UC Davis scientists and approved by the FDA

The electronic circuit of ACD provides the *electronic collimation* by selecting only those counts that are simultaneously detected by the opposite detectors, during the coincidence timing window. Typically, electronic collimation selects only 1% of the singles as prompt events for further processing, while the remaining 99% are rejected. The use of newer detector materials with digital technology and techniques has allowed all modern PET and PET/CT systems to operate in 3D mode, with substantial improvements in photon sensitivity, compared with 2D PET. Therefore, a recent trend in PET imaging is 3D mode operation, without the interplane septa, which results in improved photon sensitivity by a factor of 4–6, as compared with the 2D mode [5].

PET Imaging Modes

Following the administration of a PET radiotracer into a subject, imaging can be performed in three different modes.

A *dynamic emission scan* is used to obtain PET images in order to study the time–activity distribution of a radiotracer in a specific tissue or organ of interest. Dynamic scans are performed using a series of imaging frames, which get longer as the study progresses. Measurement of blood flow and receptor imaging studies are often performed using dynamic scans. These studies, however, may require arterial or venous sampling to provide an *input function* to estimate quantitative parameters, based on pharmacokinetic modeling of radiotracer distribution.

A *static emission scan* is normally obtained only when the radiotracer distribution is fairly stable or reaches an equilibrium state. The static scan is acquired in a single frame and it is assumed that the tracer concentration in a given tissue is constant, except for the physical decay. Most PET scans are performed 1–2 h post-administration of the dose. *Whole-body emission scan* represents a series of static scans performed at different segments or portions of the whole body. The studies are performed in several bed positions by acquiring a static scan for a specific time and then moving the patient (the bed) by a distance that is less than the axial FOV. Most clinical PET scanners have a FOV of 15–20 cm. Typically, five to seven bed positions, each requiring 3–5 min, will complete a whole-body emission scan from head to midthighs in 15–35 min. The data collected at each bed position are subsequently reconstructed into a whole-body volume and can be reoriented into *transaxial*, *coronal*, and *sagittal* views.

Continuous bed motion (CBM) PET/CT scanner has been introduced by Siemens. Unlike the conventional scanning coverage where a technologist has to decide if an additional bed is needed or not, the CBM allows for a flexible selection of the start and finish locations for each body region in the PET scan coverage. It also allows a variable motion speed and consequently the collection of optimal photon counts for each region of the body, to optimize local sensitivity.

PET Scan Reconstruction Techniques

Most current PET/CT systems employ a fully 3D iterative PET reconstruction, which allows the incorporation of CT attenuation maps as well as corrections for scatter, random events, spatial system response, and dead time. An accelerated type of iterative reconstruction, 3D ordered subset expectation maximization, can be implemented on all systems to reduce reconstruction time. Despite such implementation, 3D iterative reconstruction can still pose significant limitations with respect to processing speed in standard workstations, particularly for cardiac PET imaging using dynamic and gated protocols. More detailed discussion on PET image data correction and PET image reconstruction is beyond the scope of this chapter.

5.3.3 Small-Animal Imaging Systems

Clinical imaging systems have relatively coarse spatial resolution that is insufficient for imaging structures in small animals, which requires high spatial resolution (on the order of 1–2 mm or better). To achieve this, scanners must use higher resolution detectors and achieve finer spatial sampling (e.g., using smaller detector elements) while maintaining as high a sensitivity as possible [27–30]. Molecular imaging can be obtained by imaging techniques such as optical imaging, nuclear imaging, magnetic resonance imaging (MRI), ultrasound imaging, and computed tomography (CT) (Table 5.1). Molecular imaging techniques such as PET and SPECT provide the 3D distribution of radiopharmaceuticals and have excellent sensitivity and high resolution with excellent tissue penetration depth as shown in Table 5.3.

Table 5.3 Small imaging techniques for drug discovery and development

Technique	Resolution	Depth	Sensitivity
	mm		Moles of label detected
CT	0.05	No limit	10^{-6}–10^{-3}
Ultrasound	0.05	mm	10^{-8}–10^{-6}
MRI	0.01–0.10	No limit	10^{-9}–10^{-6}
Optical	1.0	<10 cm	10^{-12}–10^{-11}
SPECT	1–2	No limit	10^{-14}–10^{-10}
PET	1–2	No limit	10^{-15}–10^{-12}

Table modified from Jang [28]

In the late 1990s, several groups began making significant progress in the development of high-resolution small-animal PET and SPECT scanners for the study of molecular imaging techniques in several rodent disease models [31–33]. For both clinical and animal scanners, for a given size of the detector and field of view (FOV), there is a tradeoff between the resolution and the sensitivity. For example, MicroPET scanners typically have at least 10 times greater sensitivity than the microSPECT scanners. Some of the commercial animal scanners are listed in Table 5.4. Among the existing imaging modalities PET and SPECT are particularly suited for molecular imaging because there are hundreds of potential molecular imaging targets and a variety of radiolabeled probes have been developed and are currently under development. While conventional imaging yields anatomical maps or a rendering of physiologic functions, molecular imaging provides additional information on the distribution and (in some cases) amount or activity of specific molecular markers in vivo and will, thus, expand the emphasis of radiological imaging beyond the anatomical and functional level, to a molecular one.

The first animal PET tomographs designed for imaging nonhuman subjects were the SHR-2000 developed by Hamamatsu (Japan) and the ECAT-713 developed by CTI PET Systems Inc. (Knoxville, TN). The first PET system developed specifically for rodent imaging was the RATPET scanner developed by Hammersmith Hospital in collaboration with CTI PET Systems Inc. The measured spatial resolution of this scanner was found to be 2.4 mm transaxially by 4.6 mm axially, giving a volumetric resolution of 0.026 cm^3. The 3D data acquisition of that system and the high detector efficiency provided a relatively high absolute sensitivity of 4.3%. Based on the UCLA MicroPET system, Concorde Microsystems Inc. introduced the commercial MicroPET systems for primates (P4) and rodents (R4) based on a new generation of electronics designed to take full advantage of the fast decay time of the LSO detector. Since then, several other scintillator/PMT-based animal PET systems have been introduced. The Inveon, the last design of the MicroPET series, is a trimodality platform offering the largest axial extension (127 mm), up to threefold higher sensitivity (6.27%) in comparison to its predecessors There has been a significant improvement in the design of microSPECT systems for small-animal imaging studies. Because in microSPECT devices the required FOV is very small, it is possible to achieve a much higher resolution than with clinical SPECT scanners. A number of commercial systems are now available with a spatial resolution <2 mm. Some of these devices even report submillimeter resolution for specific organs and tissues that may accumulate significant amounts of radioactivity. For most of the animal SPECT scanners, the detection efficiency for high-energy photons (<200 keV) is <0.1%. As a result, it is necessary to inject radiotracers at dose levels that are hundreds of times more than the clinical doses. Many of these devices are based on a wide variety of detection instrumentation, including conventional scintillation cameras, pixelated detectors with PSPMTs or APDs, and semiconductor gamma cameras.

5.3.3.1 State-of-the-Art Preclinical PET Scanners

The remarkable improvements in system designs and overall performance introduced by the different vendors resulted in the current generation preclinical PET scanners surpassing the previous generations in many aspects. Today, high-end state-of-the-art technologies approach submillimeter spatial resolution, breaking a barrier that could open the door to more specific applications and more accurate quantification by eliminating the partial volume issue [27]. A brief summary of different commercial scanners is shown in Table 5.4 and Fig. 5.11.

Table 5.4 MicroPET scanner design characteristics and resolution

Scanner	Manufacturer	Scintillator	Crystal dimensions	Electronic	Radial FWHM (mm)	Volumetric resolution (mm^3)
MicroPET Focus 220	Siemens	LSO (12 × 12)	1.51 × 1.51 × 10	PSPMT	1.75 at 5 mm	5.35 at 5 mm
Inveon-DPET	Siemens	LSO (20 × 20)	1.51 × 1.51 × 10	PSPMT	1.63 at 5 mm	6.33 at 5 mm
Albira 3 rings	Bruker	LYSO	50 × 50 × 10	MAPMT	1.45 at center	5.55 at center
Albira	Brucker	Lyso	50 × 50 × 10	SiPMs	0.89 at center	<1 in the w-FOV
Vector	MILabs	NaI(Tl)	590 × 470 × 9.5	NA	0.6 at center	0.216 at center
PETbox4	UCLA	BGO	1.82 × 1.82.7	PSPMT	1.32 at center	3.4 at center
GNEXT	Sofie Biosciences	LYSO/BGO (8 × 8)/ (8 × 8)	1.01 × 1.01 × 61	NA	<1 at 5 mm	<1 at 5 mm
			1.01 × 1.55 × 8.9			
β-cubes	Molecules	LYSO	25 × 25 × 8	NA	1.06 at center	~1.0
Trans PET/CT X5	Raycan	LYSO (13 × 13)	1.9 × 1.9 × 13	NA	2.11 at center	5.71 at center
Nanoscan PET/CT	Mediso	LYSO (39 × 81)	1.12 × 1.12 × 13	PSPMT	1.03 at center	1.19 at center
IRIS	InviScan SAS	LYSO 27 × 26	1.6 × 1.6 × 12	NA	1.05 at 5 mm	1.38 at 5 mm

Fig. 5.11 Commercial PET, SPECT, and CT scanners for molecular imaging studies in small animals

References

1. Darambara DG, Todd-Pokropek A. Solid state detectors in nuclear medicine. Q J Nucl Med. 2002;46:3–7.
2. Ljungberg M, Pretorius H. SPECT/CT: an update on technological developments and clinical applications. Br J Radiol. 2018;90:20160402.
3. Ljungberg M. Absolute quantitation of SPECT studies. Semin Nucl Med. 2018;48:348–58.
4. Schillasi O, Orbano N. Digital PET/CT: a new intriguing for clinical nuclear medicine and personalized molecular imaging. Eur J Nucl Med Mol Imaging. 2019;46:1222–5.
5. Slomka PJ, Pan T, Germano G. Recent advances and future progress in PET instrumentation. Semin Nucl Med. 2016;46:5–19.
6. van der Meulen NP, Strobel K, Lima TVM. New radionuclides and technological advances in SPECT and PET scanners. Cancers. 2021;13:6183–98.
7. Anger HO. Scintillation camera. Rev Sci Instrum. 1958;29:27–33.
8. Erlandsson K, Kacperski K, van Gramberg D, Hutton BF. Performance evaluation of D-SPECT: a novel

SPECT system for nuclear cardiology. Phys Med Biol. 2009;54:2635–49. 6.
9. Gambhir SS, Berman DS, Ziffer J, et al. A novel high-sensitivity rapid-acquisition single-photon cardiac imaging camera. J Nucl Med. 2009;50:635–43.
10. Del Sordo S, Abbene L, Caroli E, et al. Progress in the development of CdTe and CdZnTe semiconductor radiation detectors for astrophysical and medical applications. Sensors. 2009;9:3491–526.
11. Ito T, Matsusaka Y, Onoguchi M, et al. Experimental evaluation of the GE NM/CT 870 CZT clinical SPECT system equipped with WEHR and MEHRS collimator. J Appl Clin Med Phys. 2021;22:165–77.
12. Ben-Haim S, Kennedy J, Keidar Z. Novel cadmium zinc telluride devices for myocardial perfusion imaging—Technological aspects and clinical applications. Semin Nucl Med. 2016;46:273–85.
13. Yamada Y, Nakano S, Gatate Y, et al. Feasibility of simultaneous ^{99m}Tc-tetrofosmin and ^{123}I-BMIPP dual-tracer imaging with cadmium-zinc-telluride detectors in patients undergoing primary coronary intervention for acute myocardial infarction. J Nucl Cardiol. 2021;28:187–95.
14. Weiss GJ, Korn RL. Interpretation of PET scans: do not take SUVs at face value. J Thorac Oncol. 2012;7:1744–6.
15. Lew C. Evaluating SPECT/CT quantification in clinical practice. Nuclear Medicine News & Stories. 2019. Siemens.com/NMNS.
16. Berg E, Cherry SR. Innovations in instrumentation for positron emission tomography. Semin Nucl Med. 2018;48:311–31.
17. Burnham CA, Brownell GL. A multi-crystal positron camera. IEEE Trans Nucl Sci. 1972;19(3):201–5.
18. Cherry SR, Badawi RD, Karp JS, et al. Total-body imaging: transforming the role of positron emission tomography. Sci Transl Med. 2017;9(381):eaaf6169.
19. Jones T, Townsend D. History and future technical innovation in positron emission tomography. J Med Imaging. 2017;4(1):011013, 1–17.
20. Lopez-Mora DA, Carri I, Flotats A, et al. Digital PET vs analog PET: clinical implications? Semin Nucl Med. 2022;52:302–11.
21. Nutt R. The history of positron emission tomography. Mol Imaging Biol. 2002;4(1):11–26.
22. Vandenberghe S, Moskal P, Karp JS. State of the art in total body PET. EJNMMI Phys. 2020;7:35.
23. Seo Y, Mari C, Hasegawa B. Technological development and advances in single-photon emission computed tomography/computed tomography. Semin Nucl Med. 2008;38:177–98.
24. Townsend DW. Positron emission tomography/computed tomography. Semin Nucl Med. 2008;38:152–66.
25. Levin CS. Primer on molecular imaging technology. Eur J Nucl Med Mol Imaging. 2005;32(suppl 2) S325–S345
26. van Dam HT, Seifert S, Schaart DR. The statistical distribution of the number of counted scintillation photons in digital silicon photomultipliers: model and validation. Phys Med Biol. 2012;57(15):4885.
27. Amirrashedia M, Zaidic H, Ay MR. Advances in preclinical PET instrumentation. PET Clin. 2020;15:403–26.
28. Jang B-S. MicroSPECT and MicroPET imaging of small animals for drug development. Toxicol Res. 2013;29(1):1–6.
29. Massoud TF, Gambhir SS. Integrating noninvasive molecular imaging into molecular medicine: an evolving paradigm. Trends Mol Med. 2007;13:183–91.
30. Vanderheyden JL. The use of imaging in preclinical drug development. Q J Nucl Med Mol Imaging. 2009;53:374–81.
31. Beekman FJ, van der Have F, Vastenhouw B, et al. U-SPECT-I: a novel system for submillimeter-resolution tomography with radiolabelled molecules in mice. J Nucl Med. 2005;46:1194–200.
32. Chatziioannou AF. PET scanners dedicated to molecular imaging of small animal models. Mol Imaging Biol. 2002;4(1):47–63.
33. Cherry SR. In vivo molecular and genomic imaging: new challenges for imaging physics. Phys Med Biol. 2004;49:R13–48.